The role of localization in glasses and supercooled liquids

Scott D. Bembenek and Brian B. Laird[a)]
Department of Chemistry, University of Kansas, Lawrence, Kansas 66045

(Received 26 October 1995; accepted 29 December 1995)

Localized excitations (tunneling modes, soft harmonic vibrations) are believed to play a dominant role in the thermodynamics and transport properties of glasses at low temperature. Using instantaneous normal-mode (INM) analysis, we explore the role that such localization plays in determining the behavior of such systems in the vicinity of the glass transition. Building on our previous study [Phys. Rev. Lett. **74**, 936 (1995)] we present evidence that the glass transition in two simple model systems is associated with a transition temperature below which all unstable INM's become localized. This localization transition is a possible mechanism for the change in diffusion mechanism from continuous flow to localized hopping that is believed to occur in fragile glass formers at a temperature just above T_g. © *1996 American Institute of Physics.* [S0021-9606(96)50513-3]

I. INTRODUCTION

Glasses and amorphous solids are among the most ubiquitous and technologically useful of materials. In spite of this, however, they remain poorly understood, especially in comparison to what is currently known about the thermodynamically stable condensed phases of matter: liquids and crystals. In addition to the simultaneous lack of long-range translational order and stability to shear, glasses[1] display two phenomena that distinguish them from other states of matter. First, glasses (and disordered solids, in general) exhibit thermodynamic and transport properties at very low temperatures that are markedly different than that of corresponding crystals of the same material,[2–4] indicating a much richer dynamics at low frequency. The second phenomena is the glass transition itself, defined as the temperature (or narrow temperature region) at which a supercooled liquid undergoes kinetic arrest and is no longer able to reach equilibrium, and characterized by a rapid change in slope of the thermodynamic variables such as entropy and molar volume and by a divergence of the viscosity. (The ability to make orders of magnitude changes in the viscosity with relatively small temperature change is of vital importance to the familiar art of glass blowing.) Despite recent progress, this transition remains an enigma.

At present no comprehensive microscopic theory exists that can describe the behavior of glasses over their entire temperature range. It is relatively well established now that the low temperature anomalous behavior of amorphous systems is due to the presence of disorder-induced localized excitations that coexist with and dominate the sound waves at low frequencies.[5–7] The question then arises as to whether such localization also plays a role at higher temperatures. In this paper, we use the technique of instantaneous normal mode (INM) analysis on two model systems to explore the extent to which the concept of localization can be used to describe such systems at temperatures up to and above the glass transition temperature.

The paper is organized as follows: In Sec. II, we briefly review the properties of glasses, with particular attention to the low-temperature anomalies and to the behavior near the glass transition. An introduction to instantaneous normal modes is given is Sec. III. Results for two model systems interacting with an inverse-sixth power repulsion and the Lennard-Jones potential are presented in Sec. IV and V, respectively. In Sec. VI, we conclude.

II. BACKGROUND

At very low temperatures, glasses and amorphous solids exhibit a variety of behaviors that can be said to be anomalous. For example, the heat capacity of an amorphous material below about 1 K is much greater than the corresponding crystal and has a nearly linear temperature dependence,[2] in contrast to the well-known T^3 dependence predicted by the Debye model for crystals. Also the thermal conductivity is quadratic in T (as opposed to T^3 for crystals) at very low temperatures. This anomalous behavior can be well explained by assuming that the excitations that dominate the density of states at low frequency are localized two-level states (tunneling modes).[5,6] At higher temperatures (between 1 and 20 K), this two-level state (TLS) model breaks down, failing to explain the observed plateau region of the thermal conductivity[2,3] in amorphous systems at about 10 K as well as pronounced nonlinearities in the heat capacity above 1 K.[2] Experiments[4,8] and computer simulations[9,7,10] show that, in this region, low-frequency localized harmonic modes become important.

There is some indication that the localized vibrational modes and the TLS have a common structural origin[11,12] and are associated with ''defects'' in the glass. A theory exploiting this connection has been proposed by Karpov *et al.*[13] in which the localized tunneling states and quasilocalized (resonant) low-frequency harmonic vibrational modes are described by soft anharmonic (quartic) potentials for some effective reaction coordinate. A fit using this model to experimental results on a variety of glasses yields values between 20 and 70 for the number of atoms participating in a typical

[a)]Author to whom correspondence should be addressed.

localized vibration.[11] Recent experiments also show a correlation between the nature of the glass transition and the relative concentration of TLS and the quasilocalized harmonic modes.[14,15]

When a liquid is cooled beyond its equilibrium freezing point, there are two possible events that can occur. First, the liquid can crystallize. Second, if the cooling rate is fast enough that nucleation to the crystal does not occur, then at a certain temperature the supercooled liquid will undergo a transition to a glass. It is the existence of such a transition that differentiates a glass from other amorphous solids. The glass transition is characterized by a dramatic increase in the viscosity and a sharp, but not discontinuous, change in slope of the extensive thermodynamic variables such as S,V,E (which remain continuous through the transition).[16]

The glass transition differs from a true thermodynamic transition in that the transition temperature T_g is not fixed, but is a function of the cooling rate. This implies that the glass transition is primarily kinetic in origin—at T_g most relaxation processes are frozen out and the more stable crystal phase becomes kinetically inaccessible. However, the fact that experimentally there appears to be a definite lower bound for T_g independent of the quench rate leads to the speculation that there is an underlying thermodynamics transition driving (or accompanying) the kinetic transition—this is currently a major open question.

Evidence from recent computer simulations on model glasses[17,18] has also been used to support recent speculation of the existence, in some glasses, of a dynamical transition at a temperature, T_c, *above* the glass transition temperature, where there is a change in the primary mechanism of diffusion for supercooled liquids from continuous flow to localized hopping. It has been argued[19] that this transition represents a change from a dynamical response typical of liquids to one typical of glasses, and that as such, would be a more fundamental divide than the usually defined glass transition. In the extended mode-coupling theory,[20] such a transition has been linked with the observed cross-over temperature in so-called "fragile"[21] glasses, where the temperature dependence of the viscosity changes from non-Arrhenius to Arrhenius form, but the microscopic mechanism remains unclear.

As mentioned earlier, the anomalous behavior of disordered solids at low temperatures can be well explained in terms of the existence of localized excitations. It is then natural to inquire into the role that such localization plays at higher temperatures near the glass transition—it is this question that motivates the present work.

III. INSTANTANEOUS NORMAL MODES

Instantaneous normal modes (INM)[22–24] have become a useful tool in liquid dynamics and are defined in analogy to the more familiar normal modes. For an N-particle system at a given temperature T one chooses a configuration (defined by a $3N$-dimensional vector of atomic coordinates, $\mathbf{R}_0$.) from the trajectory at some time, t_0. As in standard normal mode analysis the total potential is expanded in a Taylor series about $\mathbf{R}_0$ to yield

$$\Phi(\mathbf{R})=\Phi(\mathbf{R}_0)-\mathbf{F}\cdot(\mathbf{R}-\mathbf{R}_0)+\tfrac{1}{2}(\mathbf{R}-\mathbf{R}_0)\cdot\mathbf{K}\cdot(\mathbf{R}-\mathbf{R}_0)+\cdots, \tag{1}$$

where the $3N$-dimensional force vector, $\mathbf{F}$, and the $3N\times 3N$ dynamical matrix, $\mathbf{K}$ are given by

$$(\mathbf{F})_{i\alpha}\equiv-\left.\frac{\partial\Phi(\mathbf{R})}{\partial R_{i\alpha}}\right|_{\mathbf{R}=\mathbf{R}_0} \tag{2}$$

and

$$(\mathbf{K})_{i\alpha,j\beta}\equiv\left.\frac{\partial^2\Phi(\mathbf{R})}{\partial R_{i\alpha}\partial R_{j\beta}}\right|_{\mathbf{R}=\mathbf{R}_0}, \tag{3}$$

respectively, where i and j are atomic indices and α and β denote one of the Cartesian coordinates. Since the configuration is chosen from the trajectory of a system at nonzero temperature, it will in all probability not represent a global (or local) minimum of the potential energy surface. Therefore, unlike the case of standard normal mode analysis, the force vector cannot be assumed to vanish and the dynamical matrix is not necessarily positive definite. However, as in standard normal-mode analysis, diagonalization of the dynamical matrix to yield the instantaneous normal modes (eigenvectors) and the corresponding INM frequencies (the square roots of the INM eigenvalues) gives a description of the potential energy surface and short-time dynamics based on independent motion along the INM eigenvectors. Since the dynamical matrix can be nonpositive definite, the possibility exists to find negative eigenvalues which result in imaginary frequencies as well as the usual positive eigenvalues (positive real frequencies). In this respect, the configurationally averaged INM spectra can be viewed as giving a statistically weighted representation of the curvature of the many-body potential energy surface. For a given temperature and density, the normalized INM density of states (DOS) is defined as

$$\mathscr{D}(\omega)\equiv\left\langle\frac{1}{3N}\sum_{i=1}^{3N}\delta(\omega-\omega_i)\right\rangle, \tag{4}$$

where the $\langle\cdots\rangle$ represent a configurational average.

The INM DOS has been shown to give a good description of the short time dynamics as evidenced by calculations on the velocity correlation function (VCF).[24–29] A major question that has been the motivation for much of the work on INM's for supercooled liquids is the degree to which the INM spectra contains information about the long-time dynamics (diffusion) as well. This would seem to be a futile task, given the fact that a direct calculation of the VCF from the INM spectra diverges quite dramatically at intermediate

times. However, it has been shown that the frequency moments of the INM DOS can be used to calculate the exact t^2 and t^4 coefficients in the time series expansion of the VCF[25] and that, given a reasonable ansatz for the functional form of the VCF, knowledge of these two coefficients alone is sufficient to obtain a reasonable value for the diffusion constant in simple systems.[30]

In previous applications of INM analysis to supercooled liquids,[23,24] the imaginary frequency modes were interpreted as representing motion over a barrier and were thus termed to be ''unstable'' modes. Similarly the real frequency modes were associated with motion in a potential well and were said to represent ''stable'' modes. Using a picture due to Goldstein[31] and Zwanzig[32] in which the liquid dynamics consists of vibration about some equilibrium position (stable modes) with periodic jumps over barriers (unstable modes) to new equilibrium positions, a variety of workers,[24,25,27,33] have, with some quantitative success, developed theories showing the close relationship of the diffusion constant of a fluid to the fraction of unstable INM modes, f_u, which can be easily calculated from the INM DOS.

As we showed in our previous paper,[34] this view of supercooled liquid dynamics, although useful, is somewhat incomplete. First, not all of the imaginary frequency modes can be properly called ''unstable,'' since not all correspond to the system being near the top of a barrier, but are associated with the anharmonic shoulder of an otherwise single-well potential. As predicted by Keyes[35] and demonstrated in the present work and Ref. 34 there is a cutoff imaginary frequency below which all imaginary frequency modes are stable. Second, the close relationship of the diffusion constant to the fraction of unstable modes must break down as the glass transition is approached since the f_u is nonzero even in the glassy region where the diffusion constant is effectively zero. From this, one can infer that not all unstable modes are associated with diffusion pathways. In the next section, we will present evidence that shows that the degree to which a given unstable mode can participate in diffusional motion is intimately related to the spatial extent of the mode—that is, whether it is localized or extended.

The spatial distribution of a given INM is quantified in terms of the normalized eigenvectors, $\mathbf{e}_j^\alpha$, of each INM, where j runs over the N particles in the sample and α labels the modes. The fraction of the kinetic energy of mode α located on a given atom j is then given by $(\mathbf{e}_j^\alpha \cdot \mathbf{e}_j^\alpha)$. A standard measure of localization of mode is the participation ratio

$$p_\alpha \equiv \left[N \sum_{i=1}^{N} (\mathbf{e}_\alpha^i \cdot \mathbf{e}_\alpha^i)^2 \right]^{-1}. \tag{5}$$

For extended modes p is of order unity. For localized or quasilocalized modes, it will scale inversely with the system size. Recently, the participation ratio has been used in a study of localization of INM's in liquid water[36] in which all imaginary frequency modes were reported to be delocalized.

IV. RESULTS FOR THE INVERSE-SIXTH-POWER SYSTEM

For comparison to earlier work on the localization of normal modes at $T=0$[9,7] and our previous work on INM localization,[34] we will first discuss the results obtained for an inverse sixth-power repulsive potential

$$v(r) = \epsilon \left(\frac{\sigma}{r} \right)^6. \tag{6}$$

[In order to ensure that the potential vanishes smoothly at the chosen cutoff distance of $r_c = 3.0\sigma$, the actual potential used for the simulations was modified by the addition of $A(r/\sigma)^2 + B$, where the parameters A and B were determined by requiring that both the potential and its first derivative are zero at $r = r_c$.] In what follows the standard reduced units will the used: $r^* = r/\sigma$, $\rho^* = \rho\sigma^3$, $T^* = kT/\epsilon$, and $t^* = (\epsilon/m\sigma^2)^{1/2} t$.

The liquid and glass configurations were generated using molecular-dynamics[37] (MD) simulations. Except where otherwise indicated, the system consisted of 500 particles held at constant temperature with a reduced density of 1.0 and a reduced time step of 0.02. For the liquid systems above the glass transition temperature, T_g, the system was equilibrated at the desired temperature for 2000 time steps and configurations separated by 100 time steps were then extracted for INM analysis. For this reduced density, we estimate the T_g^* for this system to be between 0.05 and 0.08. This is lower than the estimate given in our previous paper[34] and is based on a more detailed analysis of the diffusion constants as calculated from mean-squared displacement data generated at each temperature by molecular-dynamics simulation. Figure 2 shows the diffusion constant for a range of reduced temperatures between 0.09 and 0.3 as well as fits of this data to two functional forms that have been used to model such data: the Vogel–Fulcher (VF) form

$$D = AT \exp[-B/(T - T_0)], \tag{7}$$

and a power-law form which is motivated by mode-coupling predictions[19]

$$D = C(T - T_c)^\alpha. \tag{8}$$

The VF law is best fit with $A=0.170$, $B=0.1387$, and $T_0=0.048$. The power law fit gives $B=0.237$, $\alpha=1.38$, and $T_c=0.078$. The VF form is a better overall fit based on the χ^2 value, but both are quite good. If we take the values of T_0 and T_c calculated in this manner to give lower and upper bounds for T_g we arrive at the range given above.

The glass configurations (below and near T_g) were created by quenching an equilibrated liquid to the desired temperature followed by an equilibrium run of 2000 steps. Once equilibrated, configurations separated by 100 time steps were used for data analysis. To ensure that the configuration space was adequately sampled, the quenching process was repeated after every five sampled configurations. The potential energy and radial distribution function were carefully monitored and those samples found to have undergone crystallization were removed from the data set. On the average, 80 configurations

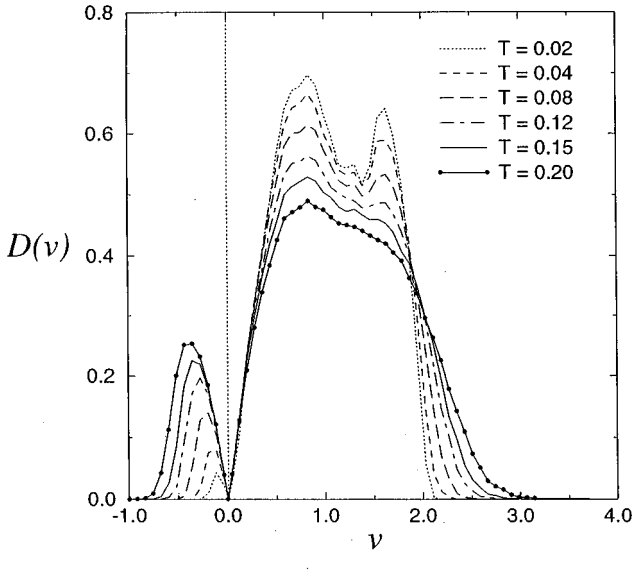

FIG. 1. The average INM density of states as a function of frequency at several temperatures for the inverse sixth-power repulsive potential. For display purposes, the imaginary frequencies are shown as negative frequencies.

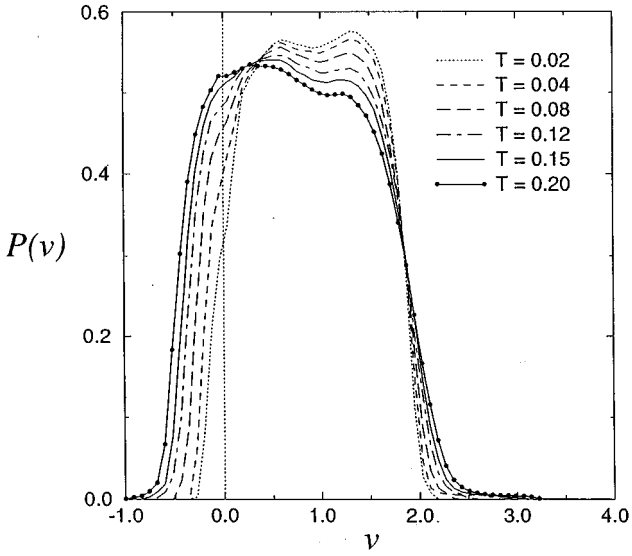

FIG. 3. The average participation ratio, $p(\nu)$, as a function of frequency for the same temperatures as shown previously for the inverse sixth DOS. Once again, the imaginary frequencies are shown as negative frequencies.

were used for each temperature, to obtain the results shown. Figure 1 shows the average INM DOS as a function of frequency for several temperatures. (It should be noted that the bimodal appearance is an artifact of the Jacobian factor used in the transformation of the eigenvalues to frequencies.[23]) As expected, the number of and average magnitude for imaginary frequencies increases with increasing temperature. Aside from this, no distinct change occurs that seems to signal that T_g has been crossed. Since this indicates that the fraction of imaginary frequency modes does not vanish even well within the glass phase, the postulated relationship between these modes and the diffusion constant must break down at low temperatures.

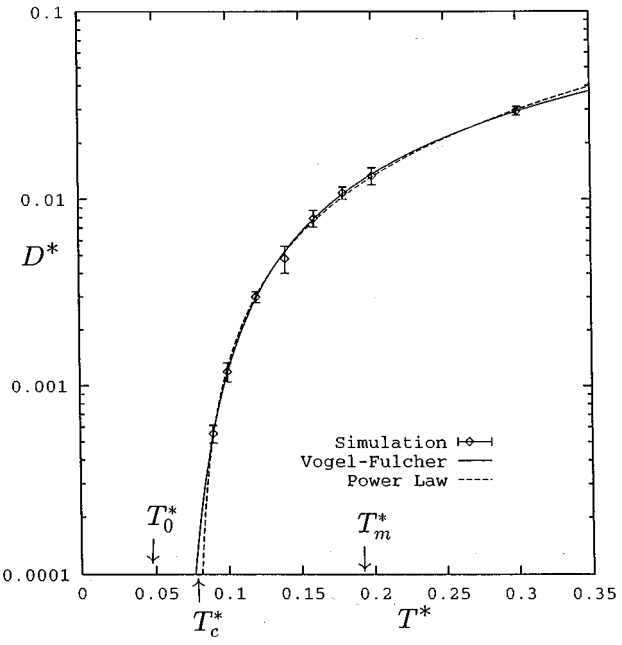

FIG. 2. Diffusion constant for the inverse sixth power fluid as a function of reduced temperature at constant density ($\rho^*=1.0$). The diamonds show the results from molecular dynamics simulation (with 2σ error bars). The solid and dotted lines are fits to a Vogel–Fulcher law $A\exp[-B/(T^*-T_0)]$ and to a power law $A(T^* - T_c^*)^{\alpha}$, respectively. For reference, the fitted T_0^* and T_c^* are indicated, as well as the melting temperature T_m^*.

As mentioned in the previous section, it has been shown that not all imaginary frequencies represent unstable modes.[34] The imaginary frequency could simply be a consequence of an inflection point at the side of an otherwise single-well region of the potential surface. Motion along such modes would not lead to a change in equilibrium position (and, therefore, could not contribute to diffusion) and should, like the real frequency modes be classified as stable. Further, the imaginary frequency may represent a mode that is localized; consequently, any barrier crossed in this configuration space direction would not lead to continuous flow but, instead, represents local rearrangement, which could still lead to diffusion, but only by a local hopping mechanism. We then divide the imaginary frequency modes in to three relevant categories: stable modes, unstable localized modes, and unstable extended modes. Thus the role of localization is very important in understanding the diffusive processes in the supercooled liquid which in turn are significant in understanding the approach to the glass transition.

Localization can be quantified using the participation ratio defined in Eq. (5). Figure 3 shows the configurationally averaged INM participation ratio, $p(\nu)$, as a function of ν, evaluated at the same set of temperatures as for the DOS. One sees a drop in the participation ratio in the tails of the eigenvalue distribution, indicating that the modes in those frequency regions are localized. This is typical of disorder-induced localization.

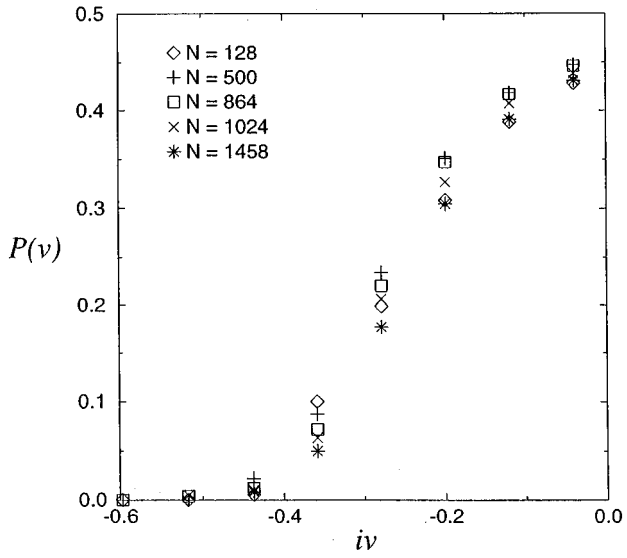

FIG. 4. The size dependence of the participation ratio (for the inverse sixth *s* system), $p(\nu)$, is shown for a temperature of 0.08 in the imaginary regime. The system sizes include: $N=128$ (diamonds), 500 (crosses), 864 (squares), 1024 (X's), and 1458 (stars). The error bars are a magnitude less than or equal to the size of the symbols, and have therefore been omitted for clarity.

In order for us to classify the modes as extended or localized, we need to establish the critical value of the participation ratio, p_c, below which a mode can be considered to be localized. This requires an analysis of the system size dependence of the participation ratio. Truly localized modes will scale inversely with system size, whereas, extended modes would show little, if any, size dependence. We can use this property to determine the value of p_c. For $T^*=0.08$ (which is our upper bound for the glass transition temperature), Fig. 4 shows the participation ratio for 5 system sizes: $N=128$, 500, 864, 1024, and 1458. In this figure, we see that the participation ratio begins to become size dependent at a critical participation ratio of about $p_c \approx 0.40$ for a 500 particle system. It should be pointed out that for localized modes the participation ratio should be ideally a monotonically decreasing function of system size. While this is true for the lowest values of $i\nu$ in Fig. 4, it is not true at some of the higher $i\nu$ values where there is still significant size dependence of p. For example, at $i\nu \approx 0.28$ we see that $N=128$ is out of order. The reason for this is that the N^{-1} scaling for localized modes is only valid when the system is much larger than the typical spatial extent of the localized modes at that frequency, thus, these results indicate that the size of the atomic clusters that make up the localized modes increases as one moves toward the center of the band. A more accurate determination of localized-to-extended crossover frequency (the ''mobility edge'') would require further analysis using much larger systems.

Determination of the stability of imaginary frequency mode requires examining the energy profiles of each INM (labeled α)

$$E_\alpha(\lambda) \equiv \Phi(\mathbf{R}_0 + \lambda \mathbf{e}_\alpha), \tag{9}$$

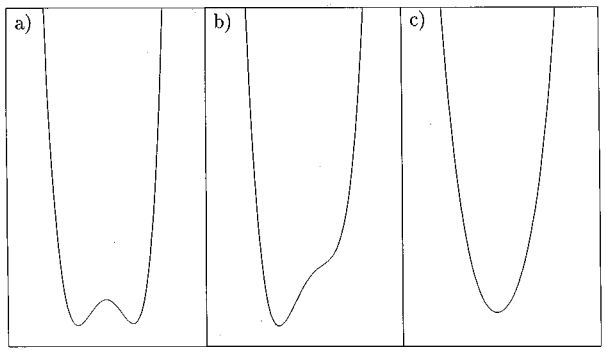

FIG. 5. Potential profiles [of $E_\alpha(\lambda)$ vs (λ)] generated from MD simulations on the inverse sixth system (at a temperature of 0.08): (a) A localized unstable mode; $p(\nu)=0.184$; $i\nu=-0.269$. (b) A stable imaginary frequency mode; $p(\nu)=0.425$; $i\nu=-0.136$. (c) An extended stable real frequency mode; $p(\nu)=0.576$; $\nu=0.236$.

where Φ is the total potential, $\mathbf{R}_0$ is the $3N$-dimensional configuration vector, $\mathbf{e}_\alpha$ is the eigenvector for mode α and λ is a parameter that varies over a predefined range and is used to advance the configuration of the system in the direction indicated by the eigenvector. Obviously, if λ is too large, the system is too far away from the initial configuration and the INM mode picture is not reliable. However, we only need a very local picture to determine the stability of a mode. In Figs. 5(a), 5(b), and 5(c) are three different potential profiles (for a temperature of 0.08) which are typical for all temperatures near T_g and represent an unstable mode, a stable imaginary frequency mode, and a stable real frequency mode, respectively.

Once the profiles for all modes have been generated and analyzed, it is possible to calculate separate densities of states for all types of modes. Figure 6 shows the unstable

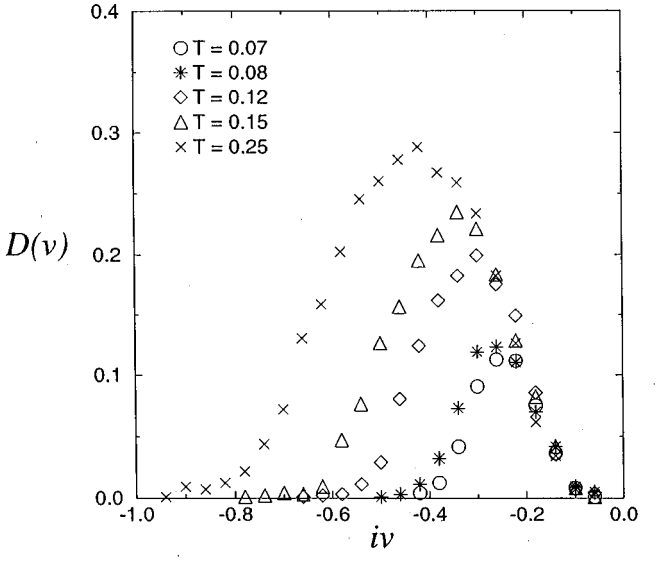

FIG. 6. The inverse sixth unstable-mode density of states for a variety of temperatures. As expected, we see that the number of unstable modes increases as the temperature increases.

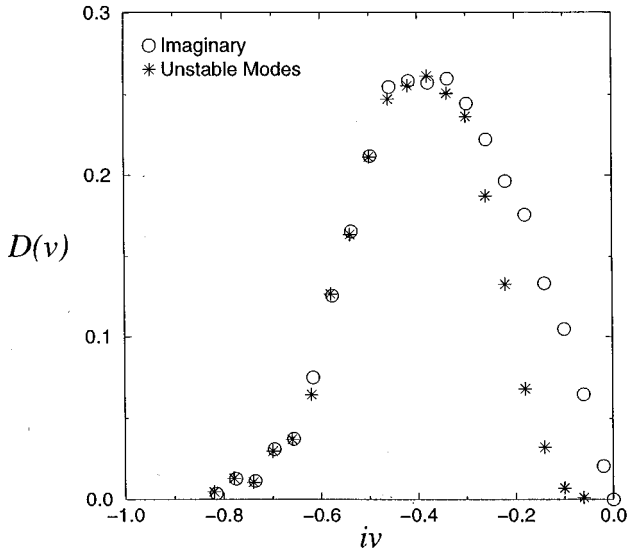

FIG. 7. The inverse sixth density of states (at a temperature of 0.20) for the imaginary frequencies and the corresponding unstable modes. As expected, the unstable mode density of states is of lesser area than that of the imaginary frequencies for a given temperature.

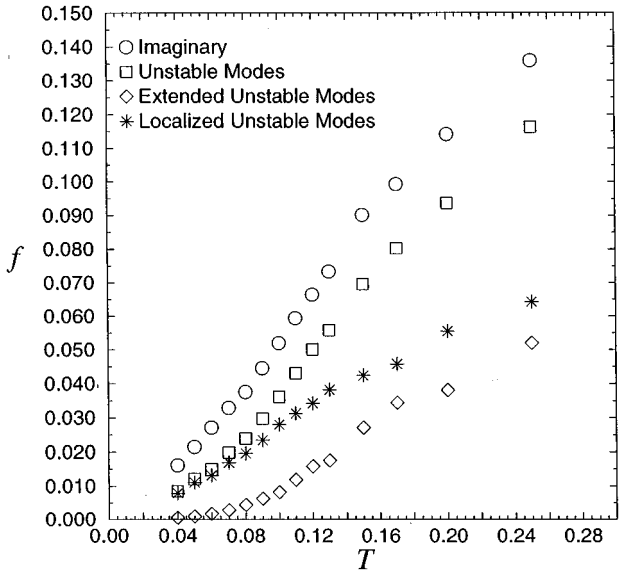

FIG. 9. Same as previous figure except with $p_c(\nu)=0.375$

mode DOS at various temperatures. Figure 7 shows the DOS for the imaginary frequencies and the corresponding unstable mode DOS for $T^*=0.20$. Using this energy profile data and a threshold of $p_c=0.40$ as a criterion for determining whether a given mode is localized, along with our profile data, we obtain the results shown in Fig. 8, where we show the fraction of the various mode types (imaginary frequency, unstable localized, and unstable extended) plotted as a function of reduced temperature. The most notable feature of this plot is that below a reduced temperature just above 0.08 the fraction of extended unstable modes becomes zero and all unstable modes are labeled as localized. Figure 9 shows the same plot with $p_c=0.375$—here, the qualitative behavior is the same with a slightly lower value for the critical temperature below which all unstable modes become localized. This provides an explanation for the observation that that below T_g there is no diffusion even though the overall fraction of unstable modes is nonzero. Below the critical temperature, diffusion could only proceed via a series of localized hops. When extended localized modes appear at higher temperatures then a continuous flow mechanism for diffusion would be possible.

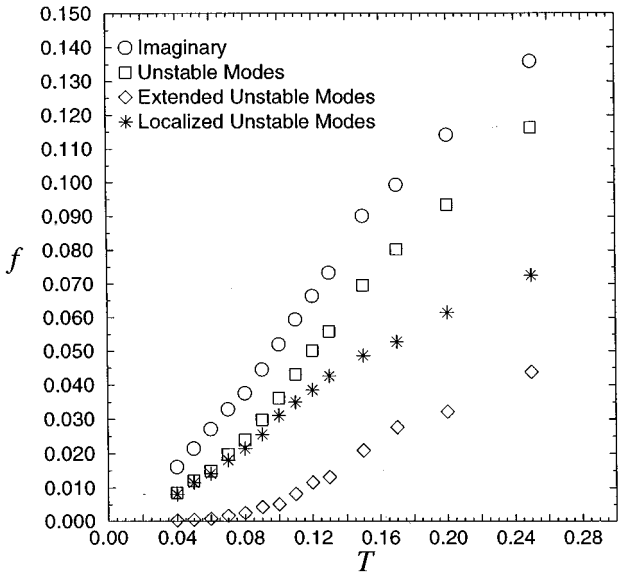

FIG. 8. Fraction of modes $[p_c(\nu)=0.40]$, for temperatures simulated on the inverse sixth system. Shown are the fractions f for the imaginary frequency modes, all unstable modes, extended unstable modes, and finally the localized unstable modes.

The dependence of the INM DOS on temperature and frequency contains information as to the distribution of barrier heights in the many-body potential surface (''energy landscape''). In a recent paper,[35] Keyes has examined the functional form of the imaginary frequency branch of the INM density of states. For a Lennard-Jones system with $\rho\sigma^3=1.0$ this part of the DOS was found to be well fit by

$$\mathscr{D}(|\omega|)=2\omega A\ \exp(-B\omega^4/T^2), \tag{10}$$

where A and B were found to be nearly constant. This form corresponds to a Gaussian distribution for the negative eigenvalues of the dynamical matrix. Vijayadamodar and Nitzan[38] have examined data for an LJ fluid at a lower density and found that this data was better fit by

$$\mathscr{D}(|\omega|)=2\omega A\ \exp(-B\omega^2/T). \tag{11}$$

We have analyzed our distributions for the inverse sixth-power potential at a variety of temperatures at fixed density and found that the low temperature data near T_g and T_m was best fit by Eq. (10) while at higher temperatures well into the liquid phase the Vijayadamodar form [Eq. (11)] was better. To illustrate this in Fig. 10 we plot $I=\ln[\mathscr{D}|\omega|/(2|\omega|)]$ vs both

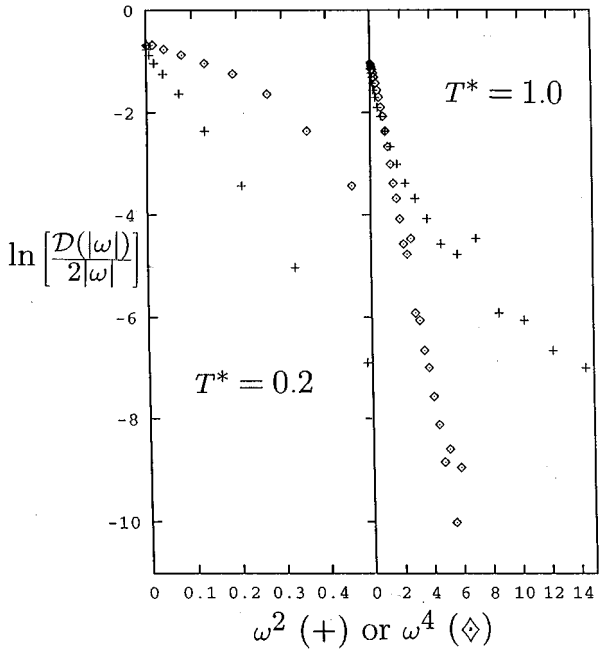

FIG. 10. $\ln[\mathcal{D}(|\omega|)/(2|\omega|)]$ for the inverse sixth power potential at two temperatures ($T^*=0.2$ and 1.0) plotted vs ω^2 and ω^4.

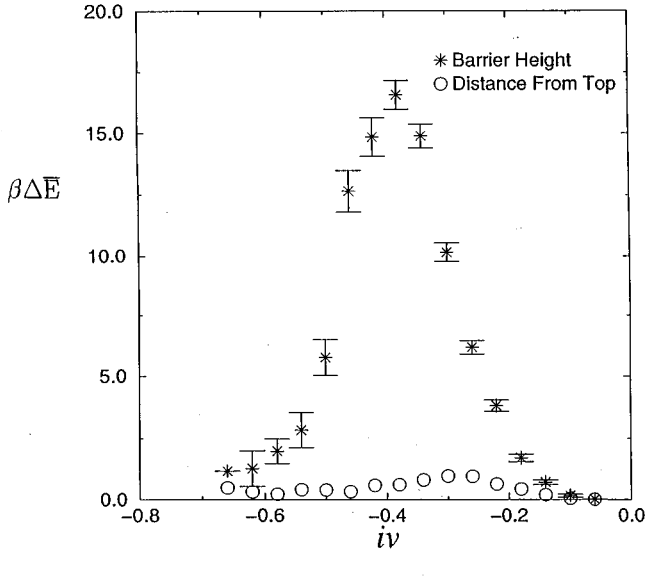

FIG. 11. Average unstable mode barrier height (stars) for the supercooled inverse sixth power fluid at a temperature of $T^*=0.12$ as a function of imaginary frequency. The circles show the average distance of the central configuration point from the top of the barrier (for this data the error bars are smaller than the size of the symbols and are omitted).

ω^2 and ω^4 for both $T^*=0.2$ and $T^*=1.0$. At the lower temperature which is slightly above the melting temperature, I is linear in ω^4 (Keyes form) whereas at the higher temperature I is linear in ω^2 (Vijayadamodar form). This is consistent with the previous results since the Vijayadamodar data was also deeper into the liquid part of the phase diagram than was the data of Keyes. This implies that the underlying potential barrier distribution is qualitatively different at low temperatures (high densities) near the glass and melting transitions than that at high temperatures (or low densities). One could speculate that this difference is due to the fact that the distributions at low temperatures are dominated by local barriers which might be expected to have a different distribution than the extended barriers that dominate the high temperature spectrum. In fact, we have shown[39] that the Keyes form is obtained when one calculates the INM density of states using the potential distribution postulated in the soft potential model of Karpov *et al.*,[11,13] for the low-frequency excitations in amorphous systems. Certainly more work needs to be done to more closely examine this question.

One of the most important quantities in the estimation of barrier crossing rates is the curvature at the top of the barrier. It is important to ask whether INM spectra can yield any information about this important quantity. In our analysis of the unstable modes and their energy profiles, it was seen that for the vast majority of modes, the system was extremely close (measured relative to the barrier height) to the top of the barrier shown by the profile for that mode. This is illustrated in Fig. 11 which shows the average unstable-mode barrier height as a function of imaginary frequency for the inverse-sixth power system at $T^*=0.12$ plotted together with the average difference between the system energy and the energy at the top of the barrier. Since higher barriers must exist, this observation implies that the INM procedure is ''fragile'' in the sense that a barrier is detected only when the system is near the top—i.e., the averaged INM spectra contains only those barriers which can be easily crossed at a given temperature. This result implies that, for the unstable modes, the INM DOS gives a relatively good estimate of the distribution of barrier-top curvature—a fact that should prove useful in using INM spectra to calculate transport properties.

V. RESULTS FOR A LENNARD-JONES SYSTEM

To make contact with the recent results of Keyes,[35] we also collected data for a Lennard-Jones system

$$v(r)=4\epsilon\left[\left(\frac{\sigma}{r}\right)^{12}-\left(\frac{\sigma}{r}\right)^{6}\right] \tag{12}$$

and will briefly summarize them here. The potential was shifted in the same manner as for the inverse sixth-power system using a cutoff of $r_c=2.5\sigma$. The same techniques that were used to obtain the previously discussed data were implemented here as well.

At a reduced density of 1.0, the glass transition was estimated by Keyes[35] to be at a reduced temperature of about 0.33–0.35. Figures 12 and 13 show the DOS and participation ratio, respectively, for several temperatures on either side of the transition—it was not possible to get data very close to the transition due to the high probability of crystallization. Here, we see the same trends as before. Figure 14 shows the unstable mode DOS for several temperatures while Fig. 15 plots the unstable modes DOS, along with imaginary mode DOS, for a temperature of 0.50. Figures 16

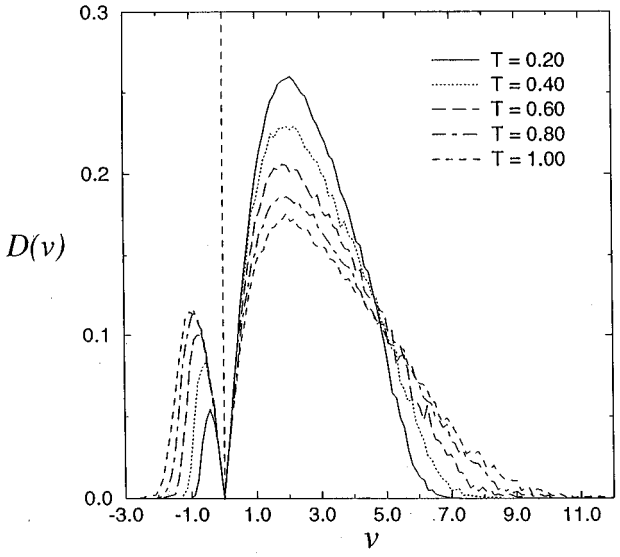

FIG. 12. The average INM density of states as a function of frequency at several temperatures for the Lennard-Jones potential. Once again, for display purposes, the imaginary frequencies are shown as negative frequencies.

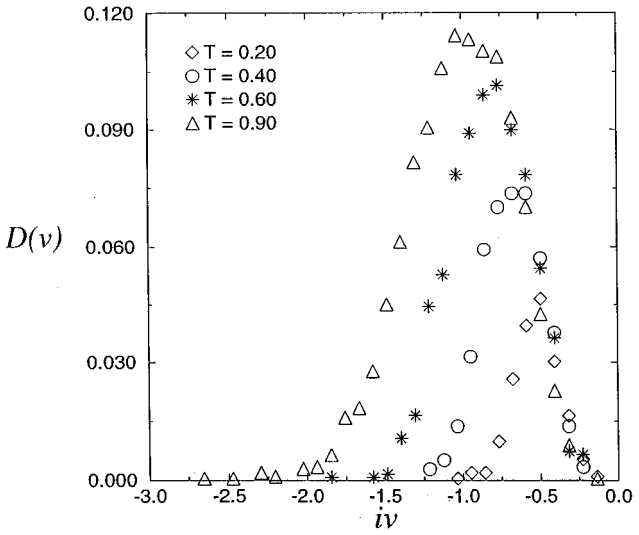

FIG. 14. The Lennard-Jones unstable-mode density of states for a variety of temperatures.

and 17 show the fraction of the various mode types using $p_c=0.40$ and 0.375, respectively. Here, we assume that the appropriate $N=500$ participation ratio for onset of localization is the same as for the inverse-sixth-power system. Again, we see that below about $T=0.35$–0.4, all unstable modes become localized. This is consistent with the value obtained for T_g, from extrapolation of diffusion data, by Keyes[35] for a Lennard-Jones system with $\rho^*=1.0$.

VI. CONCLUSION

In this work we have obtained two results concerning the structure of the trajectory-weighted potential energy surface of supercooled liquids and glasses as represented through the INM spectra. First, not all imaginary frequency modes can be termed to be unstable and are not associated with barriers. Second, once these stable imaginary frequency modes have been eliminated from the spectrum leaving only true ''unstable'' modes which are associated with barrier crossing, the unstable modes can be classified as localized or extended. As is usual in localization studies of random materials localization is confined to the edges of the DOS. The boundary between localized and extended regions of the spectra is called

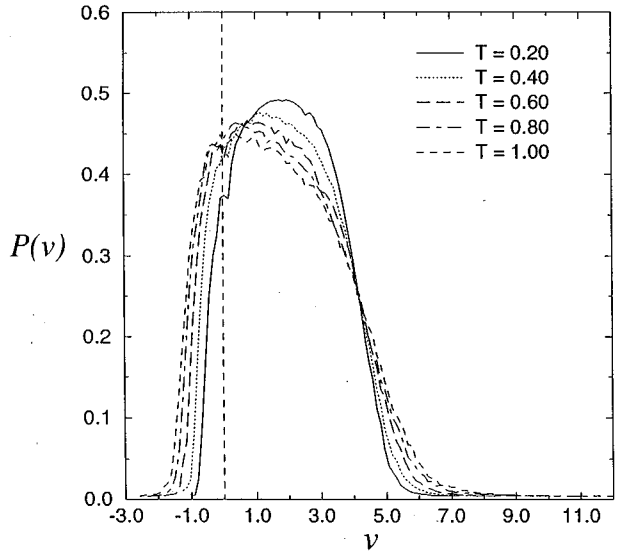

FIG. 13. The average participation ratio, $p(\nu)$, as a function of frequency for the same temperatures as shown previously for the Lennard-Jones DOS. Once again, the imaginary frequencies are shown as negative frequencies.

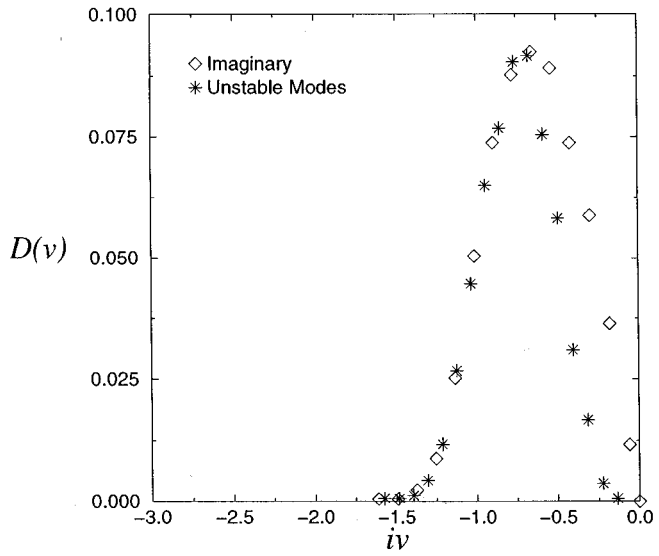

FIG. 15. The Lennard-Jones INM density of states (at a temperature of 0.50) for the imaginary frequency modes and the corresponding unstable modes.

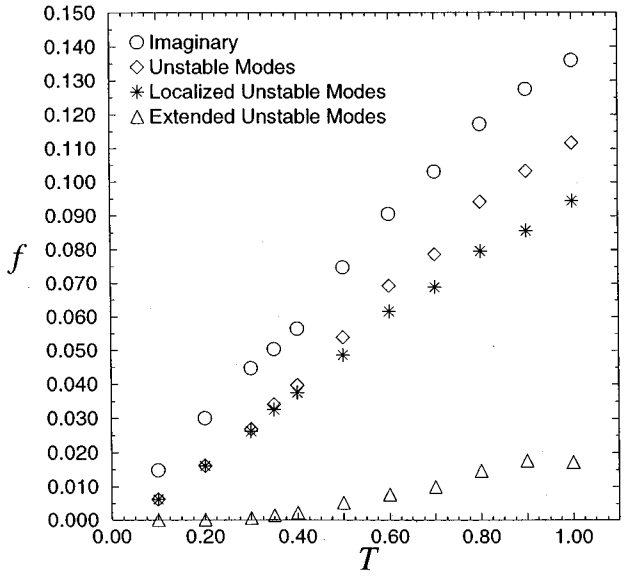

FIG. 16. Fraction of modes with $p_c(\nu)=0.40$, as a function of temperature for the Lennard-Jones system. Shown is the fraction f of imaginary frequency modes, all unstable modes, extended unstable modes, and finally the localized unstable modes.

the mobility edge. We have shown that as the temperature is lowered and the INM spectra shift toward real frequencies, the mobility edge crosses the boundary between stable and unstable modes. This indicates that there exists a temperature below which all unstable modes become localized. From our analysis this temperature is closely associated with the glass transition and we speculate that it is the origin of the proposed change in the mechanism of diffusion in fragile glasses at a temperature slightly above T_g.

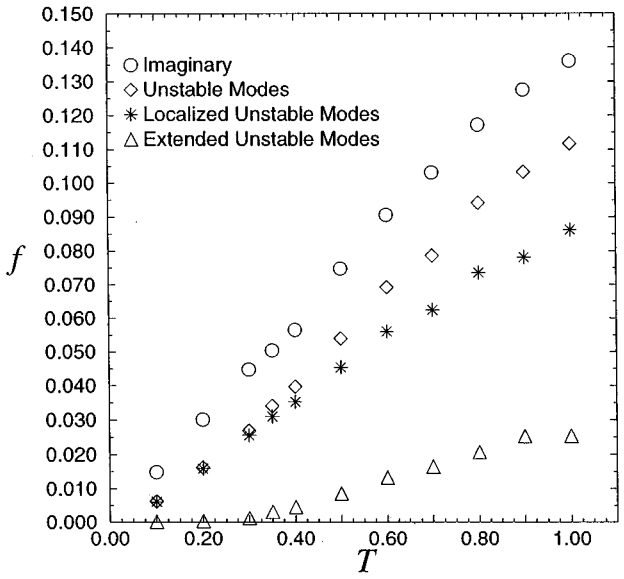

FIG. 17. Same as previous figure, except with $p_c(\nu)=0.375$.

In order to further examine the validity of this hypothesis, much more work needs to be done. First, systems of larger size should be investigated in order to get more accurate results for the ''mobility edge'' frequency separating localized and extended modes. Second, the relationship, if any, between the present results and the predictions of mode-coupling theory[19] needs to be explored since both are speculated to describe the origin of the crossover temperature in ''fragile'' glasses. Also, the INM analysis should be repeated for systems that do not display fragile behavior; i.e., strong glass formers such as SiO_2. If the localization transition discussed here is indeed the origin of the crossover temperature in fragile glasses, then the results of an analysis of the unstable modes for strong glass formers should give qualitatively different results than those presented here. Such studies are currently underway.

ACKNOWLEDGMENTS

This work has been supported by the Petroleum Research fund under Grant No. 27847-G5. We would like to thank Dr. Herbert Schober and Dr. Ulrich Buchenau for enlighting discussions and the Institute for Festkörperforschung at the Forschungszentrum in Jülich, Germany where some of these calculations were carried out.

[1] Here, we use the more restrictive definition of a glass as being an amorphous solid produced by quenching a liquid through a glass transition.
[2] R. Zeller and R. Pohl, Phys. Rev. B **4**, 2029 (1971).
[3] R. Stephens, Phys. Rev. B **8**, 2896 (1973).
[4] S. Hunklinger and A. Raychoudhuri, Prog. Low Temp. Phys. **9**, 267 (1986).
[5] P. Anderson, B. Halperin, and C. Varma, Philos. Mag. **25**, 1 (1972).
[6] W. Phillips, J. Low Temp. Phys. **7**, 351 (1972).
[7] H. Schober and B. Laird, Phys. Rev. B **44**, 6746 (1991).
[8] U. Buchenau, U. Buchenau, M. Prager, N. Nucker, A. J. Dianoux, N. Ahamad, and W. A. Phillips, Phys. Rev. B **34**, 5665 (1986).
[9] B. Laird and H. Schober, Phys. Rev. Lett. **66**, 636 (1991).
[10] J. Hafner and M. Krajci, J. Phys. Condens. Matter **6**, 4631 (1994).
[11] U. Buchenau, Y. Galperin, V. Gurevich, and H. Schober, Phys. Rev. B **43**, 5039 (1991).
[12] A. Heuer and R. Silbey, Phys. Rev. Lett. **70**, 3911 (1993).
[13] V. Karpov, M. Klinger, and F. Ignat́ev, Sov. Phys. JETP **57**, 439 (1983).
[14] A. Sokolov, A. Rosser, A. Kisliuk, and D. Quitmann, Phys. Rev. Lett. **71**, 2062 (1993).
[15] V. Malinovsky and V. Novikov, J. Phys. Condens. Matter **4**, L139 (1992).
[16] R. Zallen, *The Physics of Amorphous Systems* (Wiley, New York, 1983).
[17] J. Ullo and S. Yip, Phys. Rev. A **39**, 5877 (1989).
[18] D. Thirumalai and R. Mountain, Phys. Rev. E **47**, 479 (1993).
[19] W. Götze, in *Liquids, Freezing and the Glass Transition*, edited by D. L. J. P. Hansen and J. Zinn-Justin (North-Holland, New York, 1991), p. 287.
[20] H. Cummins, W. M. Du, M. Fuchs, W. Götze, S. Hildebrand, A. Latz, G. Li, and N. J. Tao, Phys. Rev. E **47**, 4223 (1993).
[21] A. Angell, J. Non-Cryst. Solids **73**, 1 (1985).
[22] R. Cotterill and J. Madsen, Phys. Rev. B **33**, 262 (1986).
[23] B.-C. Xu and R. Stratt, J. Chem. Phys. **92**, 1923 (1990).
[24] G. Seeley and T. Keyes, J. Chem. Phys. **91**, 5581 (1989).
[25] B. Madan, T. Keyes, and G. Seeley, J. Chem. Phys. **92**, 7565 (1990).
[26] J. Adams and R. Stratt, J. Chem. Phys. **93**, 1632 (1990).
[27] B. Madan, T. Keyes, and G. Seeley, J. Chem. Phys. **94**, 6762 (1991).
[28] G. Seeley, T. Keyes, and B. Madan, J. Chem. Phys. **95**, 3847 (1991).
[29] M. Buchner, B. Ladanyi, and R. Stratt, J. Chem. Phys. **97**, 8522 (1992).
[30] R. Sharma, K. Tankeshwar, and K. Pathak, J. Phys. Condens. Matter **7**, 537 (1995).
[31] M. Goldstein, J. Chem. Phys. **51**, 3728 (1969).
[32] R. Zwanzig, J. Chem. Phys. **79**, 4507 (1983).
[33] P. Moore and T. Keyes, J. Chem. Phys. **100**, 6709 (1994).

[34] S. Bembenek and B. Laird, Phys. Rev. Lett. **74**, 936 (1995).
[35] T. Keyes, J. Chem. Phys. **101**, 5081 (1994).
[36] M. Cho, G. R. Fleming, S. Saito, I. Ohmine, and R. Stratt, J. Chem. Phys. **100**, 6672 (1994).
[37] M. Allen and D. Tildesley, *Computer Simulation of Liquids* (Oxford Science, Oxford, 1987).
[38] G. Vijayadamodar and A. Nitzan, J. Chem. Phys. **103**, 2169 (1995).
[39] U. Zurcher and B. B. Laird (unpublished).